



HAL
open science

Hydrocarbon superhydrophobic polymers from electrochemical polymerization: an alternative to fluorine?

Mélanie Wolfs

► **To cite this version:**

Mélanie Wolfs. Hydrocarbon superhydrophobic polymers from electrochemical polymerization: an alternative to fluorine?. Material chemistry. Université Nice Sophia Antipolis, 2013. English. NNT : . tel-00933342

HAL Id: tel-00933342

<https://theses.hal.science/tel-00933342>

Submitted on 20 Jan 2014

HAL is a multi-disciplinary open access archive for the deposit and dissemination of scientific research documents, whether they are published or not. The documents may come from teaching and research institutions in France or abroad, or from public or private research centers.

L'archive ouverte pluridisciplinaire **HAL**, est destinée au dépôt et à la diffusion de documents scientifiques de niveau recherche, publiés ou non, émanant des établissements d'enseignement et de recherche français ou étrangers, des laboratoires publics ou privés.

UNIVERSITE DE NICE-SOPHIA ANTIPOLIS - UFR Sciences
Ecole Doctorale « Sciences Fondamentales et Appliquées »

T H E S E

pour obtenir le titre de

Docteur en Sciences
de l'UNIVERSITE de Nice-Sophia Antipolis

Discipline : Chimie

Présentée et soutenue par

Mélanie WOLFS

HYDROCARBON SUPERHYDROPHOBIC POLYMERS FROM ELECTROCHEMICAL POLYMERIZATION: AN ALTERNATIVE TO FLUORINE?

Thèse dirigée par le Professeur Frédéric GUITTARD et le Docteur Thierry DARMANIN

Soutenue le 13 / 12 / 2013 devant le Jury composé de

E. Magnier	Directeur de Recherches au CNRS, Institut Lavoisier de Versailles, Université de Versailles-Saint-Quentin, France	Rapporteur
V. Ravaine	Maître de Conférences - HDR, Institut des Sciences Moléculaires, Université Bordeaux 1, France	Rapporteur
F. Guittard	Professeur, Université de Nice-Sophia Antipolis, France	Directeur de thèse
T. Darmanin	Maître de Conférences, Université de Nice-Sophia Antipolis, France	Co-directeur de thèse
S. Pommeret	HDR, Président de la division Chimie-Physique de la Société Chimique de France, France	Examineur
R. Ras	Professeur, Department of Applied Physics, Aalto University, Finland	Examineur

Acknowledgments

First of all, I would like to thank Professor Frédéric Guittard for allowing me to do this PhD thesis in his research group, for his fruitful discussions about the research project but also about the doctor position. I also thank him for let me the opportunity to represent the laboratory all over the world. It was a real honor.

My thanks also go to Doctor Thierry Darmanin, co-director of this work for his involvement, his availability and his constructive discussions to move research forward together.

I would like to thank Doctor Valérie Ravaine and Doctor Emmanuel Magnier for being reviewers of this work. I also thank Doctor Stanislas Pommeret as well as Professor Robin Ras for their participation in the jury as examiners.

My thanks then go to the permanent staff of the research group: Sonia, Elisabeth but also Catherine, who was an invaluable help in the research group administration.

I sincerely thank all the members of the research group: Elena, Arnaud, Jeanne, Sabri, Cécile, Janwa, Olivier but also Abdoulaye, Chahinez, Alioune. I do not forget the past members Doctor Carine, Doctor Mamadou, Doctor Gennifer, Doctor Hervé I worked with. It was a great pleasure to work in such a good atmosphere and to share discussions, cakes, lunches and other great moments.

I would like to thank Jean-Pierre Laugier for the precious SEM images otherwise this work had not been so beautiful. It was each time a great pleasure to receive these images, synonymous of great surprises with new morphologies.

My thanks also go to the trainees I had the opportunity to supervise during these three years: Adil Jabbari, Marion Raffaldi, Florence Uvernet and Nicolas Vigneau.

Then I would like to thank Salomé and all the people I have met during my studies in Bordeaux: Morgane G., Guillaume, JP, Morgane L., Camille, Clémence, Maxime, Laura, Marie-Aline. Even if we are dispersed all over the country, it is always a pleasure to meet.

Last but not least, I sincerely thank my family: my parents, my grandparents, my little brother whose I am very proud of. A special thank finally goes to Benoît for supporting me everyday.

Table of Content

Introduction	31
Chapter 1. State of the Art on Superhydrophobic Polymers	35
I. WETTING THEORIES.....	36
II. SUPERHYDROPHOBICITY IN NATURE	40
II.1. Superhydrophobic plant surfaces.....	41
II.2. Superhydrophobic animals	43
III. FABRICATION TECHNIQUES OF SUPERHYDROPHOBIC POLYMERS.....	46
III.1. Templating or Molding	47
III.1.1. Anodic Aluminum Oxide Template	47
III.1.1.a. <u>Direct Templating.....</u>	47
III.1.1.b. <u>Template-assisted Polymerization</u>	48
III.1.2. Soft Lithography	49
III.1.2.a. <u>Natural Masters.....</u>	50
III.1.2.b. <u>Microfabrication.....</u>	50
III.1.3. Structured Hard Masters Replication.....	51
III.2. Plasma	51
III.2.1. Etching Plasma	53
III.2.2. Deposition Plasma	54
III.2.3. Sputtering.....	57
III.3. Laser	58
III.4. Polymer Self-Assembly	59
III.5. Electrochemical Polymerization	63
III.6. Electrospinning.....	66
III.7. Precipitation and Crystallization.....	71
III.8. Selective Solvent.....	73
III.9. LbL Deposition.....	75
III.10. Combination of techniques to reach superhydrophobicity.....	76

IV.	FOCUS ON FABRICATION TECHNIQUES OF SUPERHYDROPHOBIC FIBROUS	
	POLYMERS.....	77
IV.1.	Fibers Coatings.....	78
IV.1.1.	Dip-Coating.....	78
IV.1.2.	Polymerization.....	81
IV.1.3.	Other Coatings.....	83
IV.2.	Overview of the Techniques to Produce Superhydrophobic	
	Fibrous Polymers.....	84
	REFERENCES.....	88

Chapter 2. Influence of Chemical and Physical Parts onto the Wetting Properties of Linear Hydrocarbon 3,4-ethylenedioxythiophene derivatives (EDOT-Hn).....	107
I. SYNTHESIS OF MONOMERS	108
II. ELECTROPOLYMERIZATION	128
III. SURFACE CHARACTERIZATIONS.....	131
III.1. Versatile Wetting and Dewetting Surfaces.....	131
III.1.1. Surface Wettability	131
III.1.2. Surface Morphology and Roughness	133
III.2. How do the chemical and physical parts influence the surface water-repellent properties?.....	138
III.2.1. Influence of the Doping Anions	138
III.2.2. Influence of the Physical Part	139
III.2.3. Wenzel Roughness Factor and Cassie-Baxter Air Fraction.....	142
III.3. Superhydrophobic Surfaces from Short Alkyl Chain EDOT Derivatives.....	143
III.3.1. PEDOT-H6	143
III.3.2. PEDOT	146
REFERENCES.....	149
Chapter 3. Fluorocarbon vs. Hydrocarbon Polymers	151
I. EDOT-F8 vs. EDOT-HN.....	152
I.1. Monomer Synthesis.....	152
I.2. Electrochemical Polymerization	157
I.3. Surface Characterizations	158
I.3.1. Surface Wettability	160
I.3.2. Surface Morphology and Roughness	163
II. 3,4-ETHYLENEOXYTHIATHIOPHENE (EOTT) DERIVATIVES	164
II.1. Monomers Synthesis	164
II.2. Electrochemical Polymerization	195
II.3. Surface Characterizations	197
II.3.1. Surface Wettability	197

II.3.2.	Analogy in Surface Morphology.....	198
II.4.	Wettability Study of PEOTT-OFn with other Probe Liquids	203
III.	3,4-PROPYLENEDIOXYTHIOPHENE (PRODOT) DERIVATIVES.....	205
III.1.	Monomers Synthesis.....	205
III.2.	Electrochemical Polymerization	228
III.3.	Surface Characterizations.....	231
III.3.1.	Surface Wettability	231
III.3.2.	Surface Morphology.....	233
III.4.	Influence of Electrochemical Polymerization Method onto PProDOT-OF4.....	240
REFERENCES.....		245
Conclusion.....		249
Outlooks		253
Annexes		255
Annex 1: Chemical Analysis Techniques for the characterization of the Monomers		255
Annex 2: Electrochemical Polymerization Technique		256
Annex 3: Surface Characterizations Techniques.....		258
Annex 4: Experimental section - Monomer synthesis.....		260
Annex 5: Hydrocarbon conducting polymers with branched hydrophobic tail		264

List of Schemes

Chapter 2

Scheme 2-1. Synthetic way to EDOT-Hn monomers ($n = 2, 4, 6, 8, 10$ and 12).....108

Chapter 3

Scheme 3-1. Chemical route to the fluorinated 2-perfluorooctylethane-1,2-diol152

Scheme 3-2. Synthetic way to the fluorinated monomers.....152

Scheme 3-3. Synthetic way to EOTT-Fn and EOTT-Hm monomers ($n = 4, 6, 8$ and
 $m = 8, 10, 12$).....165

Scheme 3-4. Synthetic route to ProDOT-OFn and ProDOT-OHn monomers.....205

List of Figures

Introduction

- Figure 1.** Examples of chemical modifications to produce hydrophobic surfaces..... 31
- Figure 2.** Thesis synoptic representation..... 34

Chapter 1

- Figure 1-1.** Number of publications with “superhydrophobic” as enter since 1989 (Source Web of Science, October 2013)..... 35
- Figure 1-2.** Liquid droplet wetting behavior and equation of Young's state..... 36
- Figure 1-3.** Liquid droplet wetting behavior in Wenzel's state and the corresponding equation. 37
- Figure 1-4.** Liquid droplet wetting behavior in Cassie-Baxter's state and the corresponding equation. 38
- Figure 1-5.** Methods to measure the contact angle hysteresis $H = \theta_a - \theta_r$. (a) On a horizontal setup, θ_a is measured during droplet growth and θ_r is measured during its shrinkage. (b) The surface is inclined until the droplet rolls off the surface. θ_a and θ_r are measured just before the rolling occurs..... 39
- Figure 1-6.** Water droplets on a Lotus leaf (a), on the Perfoliate Knotweed leaf (c), on the Purple Setcreasea (e) and on the Rice leaf (g). SEM images of the Lotus leaf (Magnification: x 20 000) (b), of the Perfoliate Knotweed leaf (Magnification: x 10 000) (d), of the Purple Setcreasea (Magnification: x 10 000) (f) and of the Rice leaf (Magnification: x 20 000). The bars of (b), (d), (f) and (h) are 1 μm .

- The insets of (b), (d), (f) and (h) are the water contact angle on the corresponding leaves.³⁸ 41
- Figure 1-7.** Water droplets on a Ramee leaf (a) and the corresponding SEM images ((b) and (c)) with different magnifications (scale bars: 100 and 5 μm , respectively). Water droplets on a Chinese watermelon leaf (d) and the corresponding SEM images ((e) and (f)) with different magnifications (scale bars: 50 and 1 μm , respectively). Water droplets on a Silver ragwort leaf (g) and the corresponding SEM image (h and inset of (h)) with different magnifications (scale bars: 30 and 2 μm , respectively). The insets of (c) and (f) are the water contact angle on the corresponding leaf ($\theta_{\text{water}} = 164 \pm 2^\circ$ and $\theta_{\text{water}} = 159 \pm 2^\circ$, respectively). Images (a)-(f)³⁸ and Images (g)-(h).⁴⁰ 42
- Figure 1-8.** Morphology of *Salvinia molesta* floating leaf. a) Upper side of the leaf surface with a water droplet on it. (b-d) SEM images of the complex hair structures: b) Four multicellular hair grouped on top of an emergence and connected at the terminal end leading to an eggbeater-shaped structure. c) The terminal cell of each hair is collapsed forming a patch of four dead cells. d) The whole leaf surface is covered with nanoscale wax crystals (below) with exception of the terminal cells (above).²⁶ 43
- Figure 1-9.** Hierarchical micro/nano structures on the insect wings of (a) Homoptera *Meimuna opalifera* (Walker), (b) Diptera *Tabanus chrysurus* (Lowe) and (c) Termite *Nasutitermens walker* at different magnifications. Images (a-b).³⁹ Images (c).⁴⁴ 44
- Figure 1-10.** Hierarchical structuration of the gecko foot. (A) Macrostructure: ventral view of a tokay gecko (*G. gecko*) climbing vertical glass. (B) Mesostructure: ventral view of the foot, with adhesive lamellae (scansors) visible as overlapping pads. Note the clean appearance of the adhesive surface. (C) Microstructure:

	proximal portion of single lamella, with individual setae in an array visible. (D and E) Nanostructure: single seta with branched structure at upper right, terminated in hundreds of spatula tips. ⁴⁵	45
Figure 1-11.	(a) Water strider <i>Gerris</i> walking on the water surface (Scale bar: 1 mm). (b) SEM images of the hair of the water strider leg at different magnifications. ⁴⁷	46
Figure 1-12.	Overview of the techniques to fabricate superhydrophobic polymers.....	46
Figure 1-13.	SEM images of a Tokay Gecko (<i>Gekko gecko</i>) (a and c) and fabricated hierarchical PS nanohairs with high aspect ration (b and d). Inset in (b): water contact angle of the elongated hierarchical PS nanohairs. ⁵⁶	48
Figure 1-14.	Water contact angle measurements with a series of polypyrrole nanorods and Au nanoparticles after HDFT coating. Au nanoparticles size represents the diameter (d). ⁶⁵	49
Figure 1-15.	Illustration of the lotus leaf replication process and creation of a superhydrophobic surface. ⁶⁷	50
Figure 1-16.	Top-irradiation mode for the adhesion switch. The green light (530 nm, 30 mW.cm ⁻²) make the azobenzene moiety in the film into the trans state, thus the film surface shows a relatively low water adhesion. Reversibly, the UV light (365 nm, 120 mW.cm ⁻²) changes the azobenzene moiety into the cis state and the surface of the film shows a relatively high water adhesion. The time for UV and visible light was 6 and 30 s, respectively. ⁷⁸	51
Figure 1-17.	FE-SEM images of the HDPE (a-f) and PCL (g-l) replicas with micrometer-sized irregular steps (a, b, g, h) mixed structures (c, d, I, j) and nanometer-sized curled strands (e, f, k, l) replicated from Al templates etched for 10, 20, 30, 40, 50, and 60. Insets show low magnification images (x 2 000). ⁸⁶	52

- Figure 1-18.** AFM images of untreated (A) and plasma treated PTFE samples: (B) DC-bias = -575 V, $t = 700\text{s}$, $\theta_{\text{water}} = 126.2^\circ$, $R_a = 242\text{ nm}$; (C) DC-bias = -750 V, $t = 700\text{s}$, $\theta_{\text{water}} = 152.8^\circ$, $R_a = 505\text{ nm}$.⁹³ 54
- Figure 1-19.** Morphology induced by the absence (left images) or presence (right images) of the grafting step of plasma polymerization of perfluoroacrylate. AFM images (a-b) of the polymer coating (lateral scale: $5 \times 5\ \mu\text{m}$). SEM images of the polymer surface: top-view (c-d) and in cross section (e-f).¹⁰¹ 55
- Figure 1-20.** Liquid wettability of plasma polymeric film as a function of the number of plasma depositions.¹⁰² 56
- Figure 1-21.** (a) SEM images of plasma-etched PDMS after 6 min of plasma treatment. (b) AFM image of the same PDMS after a 2 min plasma treatment. (c) Image of a water droplet after hydrophobic fluorocarbon plasma. (d) AFM image of another elastomer after a 2 min plasma etching treatment.¹⁰⁷ 57
- Figure 1-22.** (a) Typical SEM images of the laser-etched PDMS surface with the convex width of about $25\ \mu\text{m}$, showing the regular arrays of microconvexes. (b) Magnified image of (a), showing the submicrometer structures on each convex. (c) High-resolution image of a single convex with width of about $50\ \mu\text{m}$ (left) and a flat PDMS surface (right).¹¹³ 58
- Figure 1-23.** SEM images of polymethylene films grown from HB + Si (a-b), HB + Ag/Au (c) and HB + Au (d) after polymerization.¹²⁰ 60
- Figure 1-24.** Shape of water droplets formed on porous and nonporous polymer layers and SEM images of the superhydrophobic porous polymers. (a) Poly(butyl methacrylate-co-ethylene dimethacrylate). (b) Poly(styrene-co-divinylbenzene).¹²² 61
- Figure 1-25.** (a) SEM images of the rambutan-like hollow polyaniline (PANI) spheres. Inset is a photograph of a rambutan.¹²⁷ (b) SEM images of the flower-like PANI

- architectures, which are composed of cross-shaped nanosheets.¹²⁹ (c) SEM images of the synthesized PANI at the polymerization time of 24h.¹³⁰ 62
- Figure 1-26.** SEM images of PProDOP-F6 with magnifications of (a) x 5 000, (b) x 25 000 and of PEDOT-F6 with magnifications of (d) x 5 000 and (e) x 25 000. (Scale bars: 1 μ m). (c) and (f): hexadecane droplets on the corresponding surface.¹⁴⁰ 64
- Figure 1-27.** Surface morphology comparison between PEOTT-F4 and PEDOT-F4, electrodeposited with the same conditions.¹⁴³ 65
- Figure 1-28.** SEM images of polypyrrole nanofibers arrays after (a) 10, (b) 20, (c) 30 and (d) 40 CV scanning cycles.¹⁵¹..... 66
- Figure 1-29.** SEM images of the electrospun PS fibers formed from 30 wt % of PS in THF/DMF solvent (1:3).¹⁸³ 68
- Figure 1-30.** SEM and TEM images of coaxially electrospun core-sheath fiber mat 1 wt % Teflon / 7 wt % PVDF. SEM images with magnifications of (a,f) x 10 000, (b) x 20 000 and (e) x 2 000 and TEM images with a magnification of (c, d) x 30 000. The difference in contrast is due to the difference of chemical structure between Teflon (core, dark) and PVDF (sheath, clear). (e, f) SEM images of core-sheath fiber sample after sheath removal.¹⁸⁶ 70
- Figure 1-31.** SEM images of *P. aeruginosa* PAO1 colonization on (A) unmodified PVC ($\theta_{\text{water}} = 80^\circ$); (B) 25 % (v/v) ethanol-treated PVC ($\theta_{\text{water}} = 113^\circ$); and (C) 35 % (v/v) ethanol-treated PVC ($\theta_{\text{water}} = 150^\circ$) samples at different incubation time points (scale bar: 10 μ m).²⁰⁴ 72
- Figure 1-32.** SEM images of the as-prepared porous film with different magnifications (Scale bars: (a) 1 μ m and (b) 100 nm).²⁰⁸ 73
- Figure 1-33.** (A-C) SEM images of 100-bilayer films fabricated from PEI and PVDMAoligo that were (A) unmodified, (B) treated with decylamine; or (C) treated with HDFFA. The images were acquired after soaking the unmodified film in water

- for 1 week and the decylamine-treated films in water for 6 weeks (Scale bars: 2 μm). (D-F) Images of water droplets (4 μL) on the corresponding surfaces.²¹⁵ 75
- Figure 1-34.** Techniques to produce Superhydrophobic Fibrous Polymers 77
- Figure 1-35.** SEM images of (a) untreated cotton textile surface and (b) cotton surface treated with 0.5 wt% amino-SiO₂, 0.5 wt% stearic acid and 0.5 vol% PFTDS. The inset of (b) is the image of static water droplets on the surface.²³¹ 79
- Figure 1-36.** Large-scale SEM image of the raw paper (a) and the magnified image of a single fiber (b). Large-scale SEM images of the fluorinated waterborne epoxy resin emulsion coated paper (c) and the magnified image of a single fiber (d). The insets in images (a) and (c) are the water droplet onto the corresponding surfaces.²³⁷ 80
- Figure 1-37.** SEM images of the surface of uncoated fabric (a) and coated surface (b). Inset is a photo of water droplet on the sample.²⁴⁷ 81
- Figure 1-38.** (a) Colored water droplets are laying onto the area of a cellulose sheet treated with PECA (defined by the red line), whereas they are absorbed by its untreated area. (c) SEM image showing the surface of a cellulose fiber roughened by submicrometer (<200 nm) PTFE particles mixed with PECA (20.0 wt% PTFE in PECA) to fabricate super water repellent cellulose sheets.²⁴⁸ 82
- Figure 1-39.** (a) Reversible wettability change of the PMETAC films by repeated counterion exchange between PFO and SCN⁻. (b) The photographs of water droplets on PMETAC brush films bearing PFO and SCN⁻ respectively, and the adhesive properties of PMETAC brush film bearing PFO.²⁵¹ 83
- Figure 1-40.** SEM images of (a) pristine cotton fiber and cotton fibers coated with (PAH-N₃/silica-N₃)_n multilayers: (b) n = 1.5, (c) n = 3.5 and (d) n = 5.5.²⁵⁶ 84
- Figure 1-41.** Synthetic route to all the monomers described in the following studies 87

Chapter 2

Figure 2-1.	Chemical structure of monomers in the present study (n = 2; 4; 6; 8; 10; 12)....	107
Figure 2-2.	Proton attribution for EDOT-H2.	110
Figure 2-3.	Carbon attribution for EDOT-H2.	111
Figure 2-4.	Proton attribution for EDOT-H4.	113
Figure 2-5.	Carbon attribution for EDOT-H4.	114
Figure 2-6.	Proton attribution for EDOT-H6.	116
Figure 2-7.	Carbon attribution for EDOT-H6.	117
Figure 2-8.	Proton attribution for EDOT-H8.	119
Figure 2-9.	Carbon attribution for EDOT-H8.	120
Figure 2-10.	Proton attribution for EDOT-H10.	122
Figure 2-11.	Carbon attribution for EDOT-H10.	123
Figure 2-12.	Proton attribution for EDOT-H12.	125
Figure 2-13.	Carbon attribution for EDOT-H12.	126
Figure 2-14.	Cyclic voltammograms of EDOT-H8 (0.01 M) on a Pt electrode recorded in 0.1 M Bu ₄ NPF ₆ /Acetonitrile with a scan rate of 20 mV.s ⁻¹	129
Figure 2-15.	Cyclic voltammogram of PEDOT-Hn with a scan rate of 20 mV.s ⁻¹ in a monomer-free solution with 0.1 M of Bu ₄ NPF ₆ /Acetonitrile.....	130
Figure 2-16.	Static contact angles of water and diiodomethane as a function of the alkyl chain length.....	132
Figure 2-17.	SEM images of a) PEDOT-H2, b) PEDOT-H4, c) PEDOT-H6 and d) PEDOT-H8 with a magnification of x 5 000 (Salt: Bu ₄ NPF ₆ ; Solvent: Acetonitrile; Q _s ≈ 200 mC.cm ⁻²).....	134

Figure 2-18.	SEM images of PEDOT-H10 (left with a magnification of a) x 250, b) x 5 000 and c) x 10 000) and PEDOT-H12 (right with a magnification of a) x 250, b) x 5 000 and c) x 10 000) (Salt: Bu_4NPF_6 ; Solvent: Acetonitrile; $Q_s \approx 200 \text{ mC.cm}^{-2}$)....	135
Figure 2-19.	Static water contact angles as a function of the deposition charge.....	137
Figure 2-20.	Mean arithmetic roughness (Ra) as a function of the deposition charge.....	137
Figure 2-21.	Wetting behavior of PEDOT-Hn series depending on their oxidation state.....	139
Figure 2-22.	SEM images of PEDOT-H10 obtained when electropolymerized in various solvents: a) propylene carbonate, b) benzonitrile, c) nitrobenzene, d) chloroform and e) dichloromethane (Magnification: x 10 000; Salt: Bu_4NPF_6 ; $Q_s = 200 \text{ mC.cm}^{-2}$).....	140
Figure 2-23.	Static water contact angle for PEDOT-H10 as a function of the deposition charge in various solvents.....	141
Figure 2-24.	Schematic representation of the influence of chemical and physical parts on the water wetting properties for PEDOT-Hn. (Salt: Bu_4NPF_6 ; $Q_s \approx 100 \text{ mC.cm}^{-2}$).	142
Figure 2-25.	SEM images of PEDOT-H6 electropolymerized with various supporting electrolyte: a) NaClO_4 , b) Bu_4NClO_4 , c) Bu_4NBF_4 , d) $\text{Bu}_4\text{NCF}_3\text{SO}_3$, e) $\text{Bu}_4\text{NC}_4\text{F}_9\text{SO}_3$ and f) $\text{Bu}_4\text{NC}_8\text{F}_{17}\text{SO}_3$ (Magnification x 5 000; solvent: Acetonitrile; $Q_s = 200 \text{ mC.cm}^{-2}$).....	145
Figure 2-26.	SEM images of PEDOT electropolymerized with two different fluorinated salts: a) $\text{Bu}_4\text{NC}_4\text{F}_9\text{SO}_3$ and b) $\text{Bu}_4\text{NC}_8\text{F}_{17}\text{SO}_3$ (Magnification x 10 000; solvent: acetonitrile; $Q_s = 200 \text{ mc.cm}^{-2}$).....	147

Chapter 3

Figure 3-1.	Chemical structure of the monomers of Chapter 3.....	151
Figure 3-2.	Protons attribution for EDOT-F8.....	153

Figure 3-3.	Carbons attribution for EDOT-F8.	154
Figure 3-4.	Fluorines attribution for EDOT-F8.	155
Figure 3-5.	Cyclic voltammograms of EDOT-F8 on a Pt electrode recorded in 0.1 M Bu ₄ NPF ₆ /acetonitrile.	158
Figure 3-6.	Influence of the deposition charge (Q _s) on the static contact angle of water (blue) and diidomethane (red) for PEDOT-F8.	159
Figure 3-7.	SEM images of the films obtained by electrodeposition of PEDOT-F8 and using different deposition charges: a) Q _s = 25 mC.cm ⁻² ; b) Q _s = 50 mC.cm ⁻² ; c) 100 mC.cm ⁻² ; d) 200 mC.cm ⁻² ; e) 300 mC.cm ⁻² (Magnification: x 5 000).	161
Figure 3-8.	AFM images of the films obtained by electrodeposition of PEDOT-F8 films at two different scales. The analyzed area are: a) 50 μm x 50 μm and b) 13 μm x 13 μm (Q _s = 100 mC.cm ⁻²).	162
Figure 3-9.	Arithmetic roughness parameter (Ra) of PEDOT-F8 as a function of the deposition charge.	163
Figure 3-10.	Proton attribution for EOTT-OH.	167
Figure 3-11.	Carbon attribution for EOTT-OH.	168
Figure 3-12.	Proton attribution for EOTT-OF4.	170
Figure 3-13.	Carbon attribution for EOTT-OF4.	171
Figure 3-14.	Fluorine attribution for EOTT-OF4.	172
Figure 3-15.	Proton attribution for EOTT-F6.	174
Figure 3-16.	Carbon attribution for EOTT-OF6.	175
Figure 3-17.	Fluorine attribution for EOTT-OF6.	176
Figure 3-18.	Proton attribution for EOTT-OF8.	178
Figure 3-19.	Carbon attribution for EOTT-OF8.	179
Figure 3-20.	Fluorine attribution for EOTT-OF8.	180
Figure 3-21.	Protons attribution for EOTT-OH4.	182

Figure 3-22.	Carbons attribution for EOTT-OH4.....	183
Figure 3-23.	Protons attribution for EOTT-OH6.....	184
Figure 3-24.	Carbons attribution for EOTT-OH6.....	185
Figure 3-25.	Protons attribution for EOTT-OH8.....	186
Figure 3-26.	Carbons attribution for EOTT-OH8.....	187
Figure 3-27.	Protons attribution for EOTT-OH10.....	189
Figure 3-28.	Carbons attribution for EOTT-OH10.....	190
Figure 3-29.	Protons attribution for EOTT-OH12.....	191
Figure 3-30.	Carbons attribution for EOTT-OH12.....	192
Figure 3-31.	Cyclic voltammogram of a) PEOTT-OF6 and b) PEOTT-OH10 (0.01 M) on a Pt electrode recorded in Bu ₄ NPF ₆ /acetonitrile with a scan rate of 20 mV.s ⁻¹ . Last voltammogram cycle of c) PEOTT-OF6 and d) PEOTT-OH10 recorded in a monomer-free solution with Bu ₄ NPF ₆ /acetonitrile.....	197
Figure 3-32.	SEM images of PEOTT derivatives substituted with various fluorocarbon or hydrocarbon chains (Magnification: x 10 000).....	200
Figure-3 33.	Optical profilometer images of a) PEOTT-OF4, b) PEOTT-OF6, c) PEOTT-OF8, d) PEOTT-OH8, e) PEOTT-OH10 and f) PEOTT-OH12. (Scale bar: from -10 (dark blue) to +20 (red) μm).....	202
Figure 3-34.	Static contact angle of water, diiodomethane and hexadecane as a function of the fluorinated chain length.....	203
Figure 3-35.	Protons attribution for ProDOT-OF4.....	207
Figure 3-36.	Carbons attribution for ProDOT-OF4.....	208
Figure 3-37.	Fluorine attribution for PEDOT-OF4.....	209
Figure 3-38.	Protons attribution for ProDOT-OF6.....	211
Figure 3-39.	Carbons attribution for ProDOT-OF6.....	212
Figure 3-40.	Fluorine attribution for ProDOT-OF6.....	213

Figure 3-41.	Protons attribution for ProDOT-OF8.....	215
Figure 3-42.	Carbons attribution for ProDOT-OF8.....	216
Figure 3-43.	Fluorine attribution for ProDOT-OF8.....	217
Figure 3-44.	Protons attribution for ProDOT-OH4.....	219
Figure 3-45.	Carbons attribution for ProDOT-OH4.....	220
Figure 3-46.	Protons attribution for ProDOT-OH6.....	221
Figure 3-47.	Carbons attribution for ProDOT-OH6.....	223
Figure 3-48.	Protons attribution for ProDOT-OH8.....	225
Figure 3-49.	Carbons attribution for ProDOT-OH8.....	226
Figure 3-50.	Cyclic voltammograms of PProDOT-OFn in a) acetonitrile and in b) dichloromethane. Cyclic voltammoogram of PProDOT-OHn in c) acetonitrile and in d) dichloromethane.....	230
Figure 3-51.	SEM images of PProDOT-OF4 in a) acetonitrile and a') in dichloromethane; PProDOT-OF6 in b) acetonitrile and b') dichloromethane; PProDOT-OF8 in c) acetonitrile and c') dichloromethane ($Q_s = 100 \text{ mC.cm}^{-2}$).....	236
Figure 3-52.	SEM images of a) PProDOT-OH4, b) PProDOT-OH6 and c) PProDOT-OH8 electrodeposited in acetonitrile (Magnification x 250. The corner insets show the zoomed-out images with a magnification of x 5 000 ($Q_s = 100$ mC.cm^{-2}))......	236
Figure 3-53.	SEM images of a) PProDOT-OH4, b) PProDOT-OH6 and c) PProDOT-OH8, electrodeposited in dichloromethane (Magnification x 10 000; $Q_s = 100 \text{ mC.cm}^{-2}$).....	237
Figure 3-54.	SEM images of PProDOT-OF4 electropolymerized in a) acetonitrile and in b) dichloromethane (Magnification x 2 500; $Q_s = 100 \text{ mC.cm}^{-2}$).....	239

Figure 3-55.	Water (blue), diiodomethane (red) and hexadecane (green) static contact angles of PProDOT-OF4 polymer films as a function of the number of scans with a scan rate of a) 0.02 V.s ⁻¹ and b) 0.1 V.s ⁻¹	240
Figure 3-56.	SEM images of PProDOT-OF4 obtained by cyclic voltammetry with a scan rate of a) 0.02 V.s ⁻¹ and b) 0.1 V.s ⁻¹ (Magnification: x 250). The corner insets show the zoomed-out images with a magnification of x 10 000 (acetonitrile; supporting electrolyte: Bu ₄ NPF ₆ ; number of scans: 10).....	242
Figure 3-57.	Arithmetic surface roughness (Ra) as a function of the scan rate and the number of CV scans.....	242

Conclusion

Figure 1.	General structures of the monomers synthesized in this work.....	249
Figure 2.	Influence of the chemical and physical part on the wetting properties for PEDOT-Hn (Q _s = 100 mC.cm ⁻²).....	250
Figure 3.	SEM images of PEOTT derivatives substituted with various fluorocarbon or hydrocarbon chains (Magnification: x 10 000).	251
Figure 4.	SEM images of superhydrophobic PProDOT-OH6 polymer films with a magnification of x 250 (left) and x 5 000 (right).....	252

Outlooks

Figure 1.	Chemical structure of the studied monomers (n = 1; 2; 3 and m = 1; 2; 3; 4; 5). .	253
------------------	---	-----

Annexes

Figure 1.	Protons attribution for EDOT-OCO-H1H1.....	265
------------------	--	-----

Figure 2.	Carbons attribution for EDOT-OCO-H1H1.	266
Figure 3.	Protons attribution for EDOT-OCO-H2H2.....	268
Figure 4.	Carbons attribution for EDOT-OCO-H2H2.	269
Figure 5.	Protons attribution for EDOT-OCO-H3H3.....	271
Figure 6.	Carbons attribution for EDOT-OCO-H3H3.	272
Figure 7.	Protons attribution for EDOT-OCO-H1H2.....	274
Figure 8.	Carbons attribution for EDOT-OCO-H1H2.	275
Figure 9.	Protons attribution for EDOT-OCO-H1H3.....	277
Figure 10.	Carbons attribution for EDOT-OCO-H1H3.	278
Figure 11.	Protons attribution for EDOT-OCO-H1H4.....	280
Figure 12.	Carbons attribution for EDOT-OCO-H1H4.	281
Figure 13.	Protons attribution for EDOT-OCO-H1H5.....	283
Figure 14.	Carbons attribution for EDOT-OCO-H1H5.	284
Figure 15.	Water contact angles of PEDOT-OCO-HnHm as a function of the deposition charge Q_s	287
Figure 16.	Arithmetic roughness (R_a) of PEDOT-OCO-HnHm as a function of the deposition charge Q_s	287
Figure 17.	SEM images of a) PEDOT-OCO-H1H1, b) PEDOT-OCO-H2H2, c) PEDOT-OCO-H3H3 with a magnification of x 250. The insets are the zoomed-out images with a magnification of x 5 000.....	288
Figure 18.	SEM images of a) PEDOT-OCO-H1H2, b) PEDOT-OCO-H1H3, c) PEDOT-OCO-H1H4 and d) PEDOT-OCO-H1H5 with a magnification of x 250. The insets are the zoomed out images with a magnification of x 5 000. ($Q_s = 200 \text{ mC.cm}^{-2}$ for images a and b; $Q_s = 100 \text{ mC.cm}^{-2}$ for images c and d).....	289

List of Tables

Chapter 1

Table 1-1.	Effect of the polymer concentration in electrospinning solution on the morphology and wettability properties. ¹⁵⁸	67
Table 1-2.	Double techniques employed in the literature to obtain superhydrophobic polymers.....	76
Table 1-3.	List of the different techniques to produce vertical or horizontal polymer fibers and the references using these techniques	85

Chapter 2

Table 2-1.	Characteristics of synthesized EDOT-Hn monomers.....	109
Table 2-2.	¹ H NMR data of EDOT-H2 in CDCl ₃	110
Table 2-3.	¹³ C NMR data of EDOT-H2 in CDCl ₃	111
Table 2-4.	MS data of EDOT-H2.....	112
Table 2-5.	¹ H NMR data of EDOT-H4 in CDCl ₃	113
Table 2-6.	¹³ C NMR data of EDOT-H4 in CDCl ₃	114
Table 2-7.	MS data of EDOT-H4.....	115
Table 2-8.	¹ H NMR data of EDOT-H6 in CDCl ₃	116
Table 2-9.	¹³ C NMR data of EDOT-H6 in CDCl ₃	117
Table 2-10.	MS data of EDOT-H6.....	118
Table 2-11.	¹ H NMR data of EDOT-H8 in CDCl ₃	119
Table 2-12.	¹³ C NMR data of EDOT-H8 in CDCl ₃	120

Table 2-13.	MS data of EDOT-H8.....	121
Table 2-14.	¹ H NMR data of EDOT-H10 in CDCl ₃	122
Table 2-15.	¹³ C NMR data of EDOT-H10 in CDCl ₃	123
Table 2-16.	MS data of EDOT-H10.....	124
Table 2-17.	¹ H NMR data of EDOT-H12 in CDCl ₃	125
Table 2-18.	¹³ C NMR data of EDOT-H12 in CDCl ₃	126
Table 2-19.	MS data of EDOT-H12.....	127
Table 2-20.	Electrochemical data for EDOT-Hn.....	128
Table 2-21.	Electrochemical data of PEDOT-Hn polymers.....	129
Table 2-22.	Static contact angles of the PEDOT-Hn films (Salt: Bu ₄ NPF ₆ ; Solvent: Acetonitrile; Q _s ≈ 100 mC.cm ⁻²).....	132
Table 2-23.	Roughness data for PEDOT-Hn (Salt: Bu ₄ NPF ₆ ; Solvent: Acetonitrile; Q _s ≈ 100 mC.cm ⁻²).....	136
Table 2-24.	Water static contact angles of PEDOT-H6 as a function of the supporting electrolyte and the deposition charge.....	144
Table 2-25.	Roughness parameters (Ra/Rq) in μm of PEDOT-H6 as a function of the supporting electrolyte and the deposition charge.....	145
Table 2-26.	Water static contact angles of PEDOT as a function of the supporting electrolyte and the deposition charge.....	146
Table 2-27.	Roughness parameters (Ra/Rq) in μm of PEDOT as a function of the supporting electrolyte and the deposition charge.....	147

Chapter 3

Table 3-1.	¹ H NMR data for EDOT-F8 in CDCl ₃	153
Table 3-2.	¹³ C NMR data for EDOT-F8 in CDCl ₃	154
Table 3-3.	¹⁹ F NMR data for EDOT-F8 in CDCl ₃	155

Table 3-4.	MS data for EDOT-F8.....	156
Table 3-5.	Dynamic contact angle of water as a function of the deposition charge.....	159
Table 3-6.	Characteristics of synthesized EOTT-OH, EOTT-OF _n and EOTT-OH _m monomers.	166
Table 3-7.	¹ H NMR data of EOTT-OH in CDCl ₃	167
Table 3-8.	¹³ C NMR data of EOTT-OH in CDCl ₃	168
Table 3-9.	MS data of EOTT-OH.....	169
Table 3-10.	¹ H NMR data of EOTT-OF ₄ in CDCl ₃	170
Table 3-11.	¹³ C NMR data of EOTT-OF ₄ in CDCl ₃	171
Table 3-12.	¹⁹ F NMR data of EOTT-OF ₄ in CDCl ₃	172
Table 3-13.	MS data of EOTT-F ₄	173
Table 3-14.	¹ H NMR data of EOTT-OF ₆ in CDCl ₃	174
Table 3-15.	¹³ C NMR data of EOTT-OF ₆ in CDCl ₃	175
Table 3-16.	¹⁹ F NMR data of EOTT-OF ₆ in CDCl ₃	176
Table 3-17.	MS data of EOTT-OF ₆	177
Table 3-18.	¹ H NMR data of EOTT-OF ₈ in CDCl ₃	178
Table 3-19.	¹³ C NMR data of EOTT-OF ₈ in CDCl ₃	179
Table 3-20.	¹⁹ F NMR data of EOTT-OF ₈ in CDCl ₃	180
Table 3-21.	MS data of EOTT-OF ₈	181
Table 3-22.	¹ H NMR data of EOTT-OH ₄ in CDCl ₃	182
Table 3-23.	¹³ C NMR data of EOTT-OH ₄ in CDCl ₃	183
Table 3-24.	¹ H NMR data of EOTT-OH ₆ in CDCl ₃	184
Table 3-25.	¹³ C NMR data of EOTT-OH ₆ in CDCl ₃	185
Table 3-26.	¹ H NMR data of EOTT-OH ₈ in CDCl ₃	186
Table 3-27.	¹³ C NMR data of EOTT-OH ₈ in CDCl ₃	187
Table 3-28.	MS data of EOTT-OH ₈	188

Table 3-29.	^1H NMR data of EOTT-OH10 in CDCl_3	189
Table 3-30.	^{13}C NMR data of EOTT-OH10 in CDCl_3	190
Table 3-31.	MS data of EOTT-OH10.....	191
Table 3-32.	^1H NMR data of EOTT-OH12 in CDCl_3	192
Table 3-33.	^{13}C NMR data of EOTT-OH12 in CDCl_3	193
Table 3-34.	MS data of EOTT-OH12.....	194
Table 3-35.	Electrochemical data of PEOOT-OFn and PEOTT-OHm polymers	195
Table 3-36.	Static and dynamic contact angles on PEOTT-Fn and PEOTT-OHm surfaces electrodeposited on gold substrate by cyclic voltammetry (salt: Bu_4NPF_6 ; solvent: acetonitrile).....	198
Table 3-37.	Roughness data for PEOTT-OFn and PEOTT-OHm polymers.....	202
Table 3-38.	Characteristics of synthesized ProDOT derivatives.....	206
Table 3-39.	^1H NMR data for ProDOT-OF4 in CDCl_3	207
Table 3-40.	^{13}C NMR data for ProDOT-OF4 in CDCl_3	208
Table 3-41.	^{19}F NMR data for ProDOT-OF4 in CDCl_3	209
Table 3-42.	MS data for ProDOT-OF4.....	210
Table 3-43.	^1H NMR data for ProDOT-OF6 in CDCl_3	211
Table 3-44.	^{13}C NMR data for ProDOT-OF6 in CDCl_3	212
Table 3-45.	^{19}F NMR data for ProDOT-OF6 in CDCl_3	213
Table 3-46.	MS data for ProDOT-OF6.....	214
Table 3-47.	^1H NMR data for ProDOT-OF8 in CDCl_3	215
Table 3-48.	^{13}C NMR data for ProDOT-OF8 in CDCl_3	216
Table 3-49.	^{19}F NMR data for ProDOT-OF8 in CDCl_3	217
Table 3-50.	MS data for ProDOT-OF8.....	218
Table 3-51.	^1H NMR data for ProDOT-OH4 in CDCl_3	219
Table 3-52.	^{13}C NMR data for ProDOT-OH4 in CDCl_3	220

Table 3-53.	MS data for ProDOT-OH4	221
Table 3-54.	^1H NMR data for ProDOT-OH6 in CDCl_3	222
Table 3-55.	^{13}C NMR data for ProDOT-OH6 in CDCl_3	223
Table 3-56.	MS data for ProDOT-OH6	224
Table 3-57.	^1H NMR data for ProDOT-OH8 in CDCl_3	225
Table 3-58.	^{13}C NMR data for ProDOT-OH8 in CDCl_3	226
Table 3-59.	MS data for ProDOT-OH8	227
Table 3-60.	Oxidation potential of the monomers (V vs. SCE) as a function of the electropolymerization solvent.....	229
Table 3-61.	Electrochemical data of PProDOT-OFn and PProDOT-OHn in acetonitrile (all potentials are in V vs. SCE).	230
Table 3-62.	Water-repellent properties of the PProDOT polymers as a function of the electropolymerization solvent for an electrodeposited charge of $Q_s = 100 \text{ mC.cm}^{-2}$	232
Table 3-63.	Diiodomethane and Hexadecane static contact angles of PProDOT-OFn polymers ($Q_s = 100 \text{ mC.cm}^{-2}$).....	233
Table 3-64.	Roughness parameters (R_a and R_q) in μm of PProDOT derivatives depending on the electropolymerized solvent.....	239

Annexes

Table 1.	Characteristics of synthesized EDOT-OCO-HnHm monomers.	268
Table 2.	^1H NMR data of EDOT-OCO-H1H1 in CDCl_3	269
Table 3.	^{13}C NMR data of EDOT-OCO-H1H1 in CDCl_3	270
Table 4.	MS data of EDOT-OCO-H1H1.	271
Table 5.	^1H NMR data of EDOT-OCO-H2H2 in CDCl_3	272
Table 6.	^{13}C NMR data of EDOT-OCO-H2H2 in CDCl_3	273

Table 7.	MS data of EDOT-OCO-H2H2.....	274
Table 8.	^1H NMR data of EDOT-OCO-H3H3 in CDCl_3	275
Table 9.	^{13}C NMR data of EDOT-OCO-H3H3 in CDCl_3	276
Table 10.	MS data of EDOT-OCO-H3H3.....	277
Table 11.	^1H NMR data of EDOT-OCO-H1H2 in CDCl_3	278
Table 12.	^{13}C NMR data of EDOT-OCO-H1H2 in CDCl_3	279
Table 13.	MS data of EDOT-OCO-H1H2.....	280
Table 14.	^1H NMR data of EDOT-OCO-H1H3 in CDCl_3	281
Table 15.	^{13}C NMR data of EDOT-OCO-H1H3 in CDCl_3	282
Table 16.	MS data of EDOT-OCO-H1H3.....	283
Table 17.	^1H NMR data of EDOT-OCO-H1H4 in CDCl_3	284
Table 18.	^{13}C NMR data of EDOT-OCO-H1H4 in CDCl_3	285
Table 19.	MS data of EDOT-OCO-H1H4.....	286
Table 20.	^1H NMR data of EDOT-OCO-H1H5 in CDCl_3	287
Table 21.	^{13}C NMR data of EDOT-OCO-H1H5 in CDCl_3	288
Table 22.	MS data of EDOT-OCO-H1H5.....	289

Glossary

AAO	Anodic Aluminum Oxide
AFM	Atomic Force Microscopy
Bu ₄ NBF ₄	Tetrabutylammonium tetrafluoroborate
Bu ₄ NC ₄ F ₉ SO ₃	Tetrabutylammonium nonafluorobutanesulfonate
Bu ₄ NC ₈ F ₁₇ SO ₃	Tetrabutylammonium heptadecafluorooctanesulfonate
Bu ₄ NCF ₃ SO ₃	Tetrabutylammonium trifluoromethanesulfonate
Bu ₄ NCIO ₄	Tetrabutylammonium perchlorate
Bu ₄ NPF ₆	Tetrabutylammonium Hexafluorophosphate
CV	Cyclic Voltammetry
d	Doublet
dd	Doublet of doublet
DMAP	4-(dimethylamino)pyridine
DMF	Dimethylformamide
E _{1/2}	Half-wave potential
ECA	ethyl-cyanoacrylate
EDC	<i>N</i> -(3-dimethylaminopropyl)- <i>N</i> '-ethylcarbodiimide hydrochloride
EDOT	3,4-Ethylenedioxythiophene
EOTT	3,4-Ethyleneoxythiathiophene
EOTT	3,4-ethyleneoxythiathiophene
E ^{ox}	Monomer oxidation potential
E _{ox, polym}	Polymer oxidation potential
E _{ox}	Monomer oxidation potential

$E_{\text{ox,opt}}$	Optimal oxidation potential
$E_{\text{red, polym}}$	Polymer Reduction Potential
GC-MS	Gas Chromatography coupled with Mass Spectroscopy
H_{liquid}	Hysteresis measured with liquid droplet
HDPE	High Density Poly(ethylene)
HFDT	Heptadecafluoro-1-decanethiol
J	Coupling Constant
LbL	Layer-by-Layer
LDPE	Low Density Poly(ethylene)
m	Multiplet
m.p.	Melting point
NaClO_4	Sodium perchlorate
NMR	Nuclear Magnetic Resonance
PAA	Poly(acrylic acid)
PAN	Polyacrylonitrile
PANI	Polyaniline
PC	Polycarbonate
PCL	Polycaprolactone
PDMS	Poly(dimethylsiloxane)
PE	Polyethylene
PECA	Poly(ethyl-cyanoacrylate)
PEDOT	poly(3,4-ethylenedioxythiophene)
PEDOT	Poly(3,4-ethylenedioxythiophene)
PEI	Poly(ethyleneimine)
PEOTT	poly(3,4-ethyleneoxythiathiophene)
PET	Polyethylene terephthalate

PFDA	Poly(heptadecafluorodecylacrylate)
PFO ⁻	Perfluorooctanoate anion
PFTDS	<i>1H,1H,2H,2H</i> -perfluorodecyltrichlorosilane
PHFMA	Poly(2,2,3,4,4,4-hexafluorobutyl methacrylate)
PMETAC	Poly[2-(methacryloyloxy)ethyltrimethylammonium chloride]
PMMA	Poly(methyl methacrylate)
PNIPAAm	Poly(N-isopropylacrylamide)
POSS	Polyhedral oligomeric silsesquioxane
PP	Poly(propylene)
PProDOT	Poly(3,4-propylenedioxythiophene)
PProDOP	Poly(3,4-propylenedioxy pyrrole)
PS	Poly(styrene)
Pt	Platinum
PTFE	Poly(tetrafluoroethylene)
pTSA	<i>p</i> -toluenesulfonic acid
PU	Polyurethane
PUA	Polyurethane acrylate
PVC	Poly(vinyl chloride)
PVDF	Poly(vinylidene fluoride)
PVDMA	Poly(2-vinyl-4,4-dimethylazlactone)
Qs	Deposition charge
r	Wenzel Roughness factor
r.t.	Retention time
R _a	Arithmetic Roughness
R _q	Root Mean Square Roughness
s	Singlet

SCE	Saturated Calomel Electrode
SEM	Scanning Electron Microscopy
sept.	Septuplet
sext.	Sextuplet
SI-ATRP	Surface-Initiated Atom Transfer Radical Polymerization
t	Triplet
TEOS	Tetraethyl orthosilicate
THF	Tetrahydrofuran
tt	Triplet of triplet
UV	Ultra-violet
α_{liquid}	Sliding angle measured for liquid
γ_{LV}	Interfacial tension between Liquid-Vapor
γ_{SL}	Interfacial tension between Solid-Liquid
γ_{SV}	Interfacial tension between Solid-Vapor
δ	Chemical shift
θ_a	Advancing angle
θ^{CB}	Apparent contact angle determined by Cassie-Baxter equation
θ_{diiodo}	Static diiodomethane contact angle
θ_r	Receding angle
θ^{W}	Apparent contact angle determined by Wenzel equation
θ_{water}	Static water contact angle
θ_{water}	Water contact angle
θ^{Y}	Contact angle of Young's equation
ϕ_a	Air Fraction
ϕ_s	Solid fraction

Introduction

From a chemist's point of view, making a hydrophobic surface is possible by using a hydrophobic bulk or by making surface modifications such as coating the surface with a polymer, activating and grafting hydrophobic molecules onto the surface, making self-assembled monolayers onto the surface or depositing self-assembled monolayers or hyperbranched polymers for example (Figure 1). With all these techniques, hydrophobic surfaces are mainly flat.

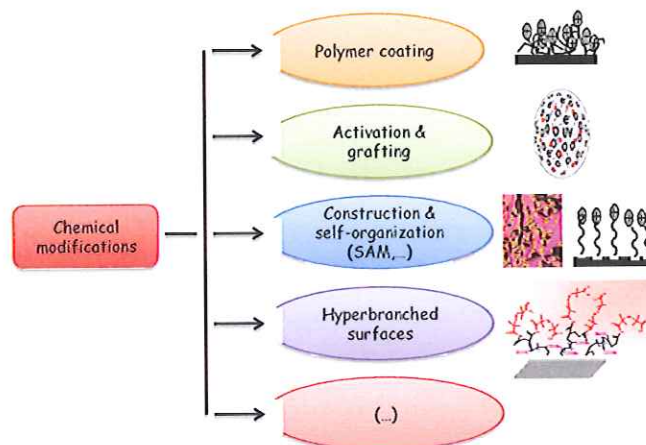


Figure 1. Examples of chemical modifications to produce hydrophobic surfaces.

The hydrophobicity comes from the intrinsic hydrophobicity of the bulk or the deposited species. The water-repellency is evaluated by measuring the contact

angle between the water droplet's tangent and the solid surface's tangent. With these techniques described in Figure 1, the highest water contact angle we could obtain was 120° which corresponds to the smooth surface of poly(tetrafluoroethylene) (PTFE). In 2000, Genzer and his co-workers previously stretched their surface before grafting a self-assembled monolayer of fluorinated compounds (Genzer, J; Efimenko, K. *Science* **2000**, *290*, 2130-2133). From this technique, they deposited a mechanically assembled monolayer (MAM) instead of a self-assembled monolayer (SAM). Thus, they enhanced the density of the grafted molecules and they increased the water-repellency with a water contact angle of 130 - 135° .

Fluorinated compounds are often employed to fabricate hydrophobic surface. The advantages are their chemical and thermal inertia as well as their low surface energy. However due to their chemical inertia, long fluorinated tails are not easily degradable. As a consequence, it is very difficult or quasi impossible for the body of living species to eliminate these compounds. Long fluorinated tails are thus considered as bioaccumulable species. In opposition to synthetic pathway proposed in literature, in nature, we can find surfaces with extreme water-repellency properties (i.e. on which water droplets remained spherical) without

using fluorine chemistry. These surfaces are named superhydrophobic. This phenomenon could be explained by an appropriate combination of either morphology, either roughness or surface structuration and low surface energy raw materials. Hence, the main subject of this research work was to find alternative to fluorine chemistry by the preparation of superhydrophobic material within hydrocarbon series.

In literature, several techniques to produce superhydrophobic surfaces have been described. Amongst them, electrochemical polymerization allowed the design of surfaces with special wettability and especially the possibility to obtain superhydrophobic surfaces. The main advantages of this technique are:

- The speed: the deposition and the surface structuration occur at the same time
- The versatility: an accurate design of the monomer chemical structure influences the resultant morphology and properties. It is also possible to control the morphology through the electrochemical parameters (deposition charge, supporting electrolyte, solvent, deposition technique, etc)

In this thesis, the challenges were:

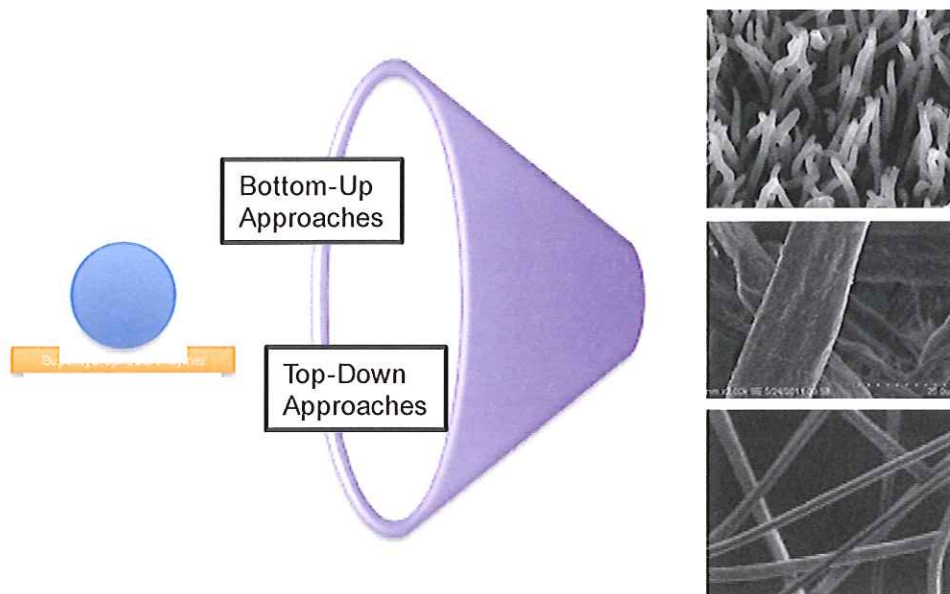
1. To make an assessment of the existed techniques to produce superhydrophobic surfaces with polymer material
2. To focus on superhydrophobic fibrous polymers since fibers present many practical applications
3. To produce superhydrophobic surfaces with hydrocarbon conducting polymers
4. To evaluate the influence of chemical and physical part onto the wetting properties
5. To compare hydrocarbon conducting polymers with fluorinated analogues
6. To study the impact of the polymerizable core onto the properties.

All these challenges can be summed up in Figure 2.

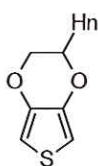
This work is thus divided into four chapters. First, we will present a review of the techniques employed to obtain superhydrophobic polymers then superhydrophobic fibrous polymer surfaces. The second chapter is devoted to one particular hydrocarbon ethylenedioxythiophene (EDOT) series. We will see if superhydrophobicity could be reached with these polymers and if we can get chemical and physical parts impacting onto the wetting properties. Finally, the fourth chapter will describe the surfaces properties comparison between

hydrocarbon and fluorinated surfaces as well as the influence of polymerizable core onto the resultant surface properties.

Chap. 1

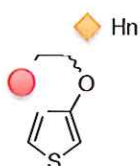


Chap. 2



- Superhydrophobicity with Hydrocarbon conducting polymers?
- % of Chemistry and Physics onto Contact angle?

Chap. 3



- Hn vs. Fn
- Influence of Polymerizable core?

Figure 2. Thesis synoptic representation.